https://doi.org/10.5194/amt-2020-65
Preprint. Discussion started: 27 May 2020

Atmospheric Measurement Techniques Discussions

Measurements of Ozone Deposition to a Coastal Sea by Eddy Covariance

David C. Loades[1], Mingxi Yang[2], Thomas G. Bell[2], Adam R. Vaughan[1], Ryan J. Pound[1], Stefan Metzger[3,4], James D. Lee[4,5] & Lucy J. Carpenter[1]

[1]Wolfson Atmospheric Chemistry Laboratories, Department of Chemistry, University of York, University Road, York, YO10 5DD, UK
[2]Plymouth Marine Laboratory, Prospect Place, Plymouth, PL1 3DH, UK
[3]National Ecological Observatory Network Program, Battelle, 1685 38th Street, Boulder, CO 80301, USA
[4]Department of Atmospheric and Oceanic Sciences, University of Wisconsin-Madison, 1225 West Dayton Street, Madison, WI 53706, USA
[5]National Centre for Atmospheric Science, University of York, University Road, York, YO10 5DD, UK

Correspondence to: David C. Loades (dl823@york.ac.uk)

Abstract. A fast response (10 Hz) chemiluminescence detector for ozone (O_3) was used to determine O_3 fluxes using the eddy covariance technique at the Penlee Point Atmospheric Observatory on the south coast of the UK during April and May 2018. The median O_3 flux was -0.132 mg m^{-2} h^{-1} (0.018 ppbv m s^{-1}) corresponding to a deposition velocity of 0.037 cm s^{-1} (interquartile range 0.017–0.065 cm s^{-1}) – similar to the higher values previously reported for open ocean flux measurements, but not as high as some other coastal results. Eddy covariance footprint analysis of the site indicates that the flux footprint was predominantly over water (> 96%), varying slightly with tide. At moderate-to-high wind speeds, ozone deposition increased with wind speed, and showed a linear dependence with friction velocity of comparable magnitude to predictions from the one-layer model of (Fairall et al., 2007). Deposition was also elevated at very low wind speeds, most likely because the footprint contracted to include a greater land contribution in these conditions.

1 Introduction

Tropospheric ozone is important due to its considerable effects on human health (Medina-Ramón et al., 2006), agricultural yields (Heck et al., 1982) and global warming (Stevenson et al., 2013). Dry deposition is a major sink of tropospheric ozone, comprising around 25% of total loss from the troposphere (Lelieveld and Dentener, 2000; Pound et al., 2019). Deposition to the sea surface is the greatest source of uncertainty in global estimates of total ozone dry deposition (Hardacre et al., 2015) due to deposition occurring at a slow and highly uncertain rate, but over a vast area. Despite this, there are few reported observations of ozone deposition to the sea surface.

Early work to determine oceanic O_3 deposition was either laboratory-based (Garland et al, 1980; McKay et al., 1992) or used box enclosure loss rate experiments in the field (Aldaz, 1969; Galbally and Roy, 1980). Such experiments determined atmospheric and surface resistance values for ozone deposition, but do not accurately represent real world physical processes

https://doi.org/10.5194/amt-2020-65
Preprint. Discussion started: 27 May 2020


Atmospheric Measurement Techniques Discussions

such as turbulence at the air/sea interface. More recent flux measurements have been made with the eddy covariance method, which is the best way of observing fluxes in a system without perturbing it. Eddy covariance measurements have been made from coastal towers (Gallagher et al., 2001; Whitehead et al., 2009; McVeigh et al., 2010), aircraft (Lenschow et al., 1982; Kawa and Pearson, 1989), and ships (Bariteau et al., 2010; Helmig et al., 2012). The reported deposition velocities (v_d) over saltwater vary greatly: 0.01–0.15 cm s^{-1}, with windspeed dependencies evident in some measurements and absent from others.

The reported eddy covariance measurements use two different techniques to measure ozone at high frequency, both utilising chemiluminescent reactions of ozone. In the instruments used for tower-based measurements (Gallagher et al., 2001; McVeigh et al., 2010; Whitehead et al., 2009), ozone is reacted with a coumarin-based dye on the surface of a silica gel disk. Aircraft (Kawa and Pearson, 1989; Lenschow et al., 1982) and ship-borne (Bariteau et al., 2010; Helmig et al., 2012) instruments have instead reacted ozone with gas phase nitric oxide.

Ozone deposition is likely to depend both upon physical exchange, facilitated by diffusion and turbulence, and chemical reaction at the water's surface (Chang et al., 2004; Fairall et al., 2007; Luhar et al., 2018). Iodide in sea water has been identified as a key reactant (Garland et al., 1980), and there has been considerable recent progress in understanding its global distribution (Chance et al., 2014; Macdonald et al., 2014; Sherwen et al., 2019). However, there has only been one report of the dependence of the iodide – ozone rate constant with temperature (Magi et al., 1997), and this remains a considerable uncertainty in global models. Dissolved organic material (DOM) has been suggested to be of similar importance to ozone deposition as iodide (Martino et al., 2012; Shaw and Carpenter, 2013), especially given its enrichment in the sea surface microlayer (SML) (Zhou and Mopper, 1997). The complex and variable composition of DOM makes assessing its global reactivity towards ozone a challenge.

A better characterised ozone deposition sink to the oceans would significantly improve our understanding of global tropospheric O_3 cycling. Here we present coastal ozone flux measurements made at Penlee Point Atmospheric Observatory (PPAO; https://www.westernchannelobservatory.org.uk/penlee/) on the southwest coast of the UK using a fast response gas phase chemiluminescence detector (CLD). Causes of natural variability and uncertainty in the observed deposition velocity are discussed, including the effects of the changing relative contributions from sea and land within the flux footprint.

2 Experimental

2.1 Measurement location

The PPAO is on a headland just south-west of Plymouth, UK, located 50° 19.08' N, 4° 11.35' W. The observatory is located 11 m a.m.s.l. with an extendable mast. It lies 30–60 m away from the sea, depending on tide, with the intervening land predominantly bare rock with some grass immediately surrounding the tower. For the work presented here, the top of the tower was extended to 19 m a.m.s.l. The dominant wind directions are from the south-west, followed by the north-east

https://doi.org/10.5194/amt-2020-65
Preprint. Discussion started: 27 May 2020


Atmospheric Measurement Techniques Discussions

(Figure 1). The focus of this work is the south-west (180–240°) wind sector, which brings in air from the Atlantic Ocean and English Channel to the site (Yang et al., 2016).

2.2 Experimental set-up

The ozone chemiluminescence detector was adapted from an Eco Physics® CLD 886 NO_x detector, working on the same principle as the instrument used by Helmig et al. (2012). A supply of excess NO is introduced to the sample, which reacts with O_3 to generate NO_2 in an excited state. The relaxation process leads to emission of a photon that is amplified and detected using a photomultiplier tube (PMT). In order to maintain a low number of dark counts, the PMT is cooled to -5°C by a Peltier cooler. Clean dry air is continuously pumped over the PMT to avoid the build-up of water (Figure 2).

Sample air was drawn from the top of the tower through ~10 m of 3/8'' PFA tubing by a vacuum pump at 13.5 L min^{-1}. This maintained a turbulent flow in the main sampling line (Reynolds number = 3000). A flow of 300 mL min^{-1} was drawn from this sample manifold through 1/8'' PFA tubing and into the analyser using an internal vacuum pump (Figure 2 part 11), limited by a critical orifice (part 5). Before entering the analyser, the sample air was first passed through a dryer (part 3) consisting of 60 cm of Nafion tubing coiled in a container of desiccant (indicating Drierite) to reduce humidity. A three-way solenoid valve (part 2) allowed for a sample of indoor air passed through a charcoal filter (part 1) to remove O_3 to record an instrument zero. A 50 mL min^{-1} flow of 2% NO in N_2 was supplied separately to the analyser at a pressure of 4 bar through approximately 1.5 m of 1/8'' PFA tubing. The NO and O_3 were then mixed immediately before the reaction chamber (part 9, at ~26 mbar pressure) and the resulting chemiluminescence was detected by the PMT.

The CLD counts were logged at 10 Hz and converted into ozone mixing ratios using the signal from a co-located, recently calibrated 2B model 205 dual beam ozone monitor. The CLD sensitivity was determined to be 240 counts s^{-1} $ppbv^{-1}$ and showed no obvious dependence on humidity (Figure 3) providing evidence for the efficacy of the dryer. Instrument dark counts were 480±40 count s^{-1}, leading to a 10 Hz signal-to-noise ratio of 33 for the average 46 ppbv O_3 measured during this work.

Three-dimensional wind data were obtained from a Gill WindMaster Pro 3D sonic anemometer at 10 Hz. Humidity, air pressure and temperature data were logged at 0.25 Hz from a Gill MetPak Pro. Vertical wind data were adjusted by +16.6% and +28.9% in magnitude for positive and negative values, respectively, in line with the corrections recommended for a reported firmware bug in the Gill WindMaster instruments: (http://gillinstruments.com/data/manuals/KN1509_WindMaster_WBug_info.pdf).

3 Pre-flux processing

The eddy covariance method (EC) relies on the simultaneous measurement of vertical wind speed (w) and the relevant scalar (in this case, ozone concentration). These values were determined at 10 Hz in order to resolve the full range of eddies responsible for vertical ozone transport. It is necessary to average data over a suitable period to reduce random noise and

https://doi.org/10.5194/amt-2020-65
Preprint. Discussion started: 27 May 2020


Atmospheric Measurement Techniques Discussions

capture transport from large eddies, whilst avoiding too long a period such that non-turbulent transport and non-stationarity become issues. An averaging time of around 30 minutes is often recommended (Foken, 2008). Previous measurements of O_3 flux have used averaging periods from 10 minutes (Helmig et al., 2012) to 1 hour (Gallagher et al., 2001), and a 20-minute period was chosen for this work. Prior to the flux calculation, data were despiked using a median filter despiking method (Brock, 1986; Starkenburg et al., 2016) using an order of N = 4 (9 points in a window). This involves binning the differences from the normalised data into exponentially more bins until bins exist within the range of the histogram that have zero values. Difference values beyond these empty bins are then identified as spikes and removed. For the flux calculation, data were linearly detrended to determine deviation from the mean within the averaging period. A double rotation was applied to the wind data in each averaging period to align the u axis with the mean wind and remove any tilt in the wind vector, resulting in a mean vertical wind of zero.

Due to the Nafion dryer and the fixed temperature and pressure of the reaction chamber, density corrections known as WPL corrections (Webb et al., 1980) were unnecessary for However, the presence of water vapour was taken into account for the determination of ancillary parameters such as the Obukhov length used in footprint modelling. It should be noted that beyond its effect on mixing ratio, water vapour also quenches the chemiluminescence of the reaction of NO with O_3. This can be dealt with either by determining the instrument sensitivity over a range of water vapor conditions (at the cost of some sensitivity) and applying a correction, or by sufficiently drying the sample air. The latter approach was taken here. Despite a range of humidity (2.8×10^{-5}–1.8×10^{-2} mol/mol, Figure 3) over the 42-day observation period, the two instruments compare well when using a fixed sensitivity for the CLD. The sensitivity value of 240 ppbv s^{-1} also compares favourably to 213 ppbv s^{-1}, which was estimated using a supply of dry ozone during lab tests prior to deployment. These results suggest that the dryer removed any major effect on the detection of ozone concentration and flux.

The sample air must travel from the inlet to the detector through the inlet, which introduces a time lag relative to the instantaneously measured wind data. The two datasets must therefore be realigned in order to calculate the covariance. A cross-correlation function (CCF) was calculated at different time lags, with a high-pass Butterworth filter applied to the input values. The presence of a negative peak in the resulting CCF spectrum indicated a strong anticorrelation between ozone concentration and vertical wind, characteristic of deposition. Individual CCF plots were noisy, and gave scattered lag values, with a high density around 4 seconds. Daily average CCF plots indicated clear peaks in all but one case and drifted from 3.9 to 4.1 seconds over the course of the experiment (e.g. Figure 4). This is likely a consequence of slight particulate build-up in the sample line filters over the course of the measurements. Individual 20-minute flux interval lags were accepted if they fell between 3.5 and 4.5 seconds to allow for some variability in conditions, vacuum pump strength etc. Lags that fell outside of these boundaries were then set to a value determined by a linear fit of the accepted data (Figure 5). Simply setting the lag to 4 seconds in all instances was found to decrease the flux by 5% relative to the method used here (CCF lag determination maximises the flux magnitude). The expected lag was also estimated from the inlet setup: a 13.5 L min^{-1} flow rate through 10 m of 3/8'' tubing plus a 300 mL min^{-1} sample flow through 2 m of 1/8'' tubing yields a 4.2 second lag, similar to the CCF-determined values.

https://doi.org/10.5194/amt-2020-65
Preprint. Discussion started: 27 May 2020


Atmospheric Measurement Techniques Discussions

Following these steps, the ozone flux was calculated on a 20-minute basis using eddy4R (Metzger et al., 2017) with a modified workflow. Flux values were then used to determine the deposition velocity according to Eq. (1):

$$v_d = \frac{F}{[O_3]} \quad (1)$$

where v_d is deposition velocity in cm s^{-1}, F is flux in mol cm^{-2} s^{-1}, and $[O_3]$ is ozone concentration in mol cm^{-3}. Molar flux was calculated using the instantaneous vertical wind, ozone mixing ratio and density of dry air. Similarly, the ozone concentration used in Eq. (1) was calculated for dry air using the mean ozone mixing ratio for the averaging period to avoid introducing a dependence on water vapour to the deposition velocity.

4 Data selection

A series of selection criteria were applied to the calculated 20-minute flux data. Firstly, periods with more than 10% missing data were excluded. Missing data were most commonly caused by periods of maintenance, or when heavy rain disrupted the sonic anemometer readings. Data were also selected by wind direction – only data between the true wind direction of 180° and 240° were accepted to avoid observing deposition on the headland to the north-west.

A selection criterion based on ozone variation, as used by Bariteau et al. (2010), was introduced to avoid periods of non-stationarity i.e. significantly different conditions within an averaging period (such as a sudden change in the air mass passing by the sensor, or a change in wind direction). Data were excluded if the ozone concentration drifted significantly (> 6 ppbv in 20 minutes) or if the standard deviation in ozone was above 2 ppbv. Data with a standard deviation in wind direction of > 10° were also removed to avoid non-stationarity of wind, as performed by Yang et al., (2016) for the same site. We note that the discontinuity in wind direction at for northerly winds (360°–0°) can incorrectly increase the standard deviation measured near to north. However, this issue does not arise as we consider only winds from the south-westerly sector.

Periods of low wind speed were also excluded because of suspected land influence, as indicated by elevated deposition velocities (see Sect. 5). This is contrary to the trend of increasing deposition with wind speed proposed by Chang et al. (2004) and observed during open ocean cruises by Helmig et al. (2012). Yang et al. (2016, 2019) observed a similar enhancement in CO_2 transfer at wind speeds, and chose to filter out data when wind speeds were < 5 m s^{-1}. Footprint analysis was used to investigate the potential for land influence within the footprint area. Land influence may increase as the footprint contracts at low wind speeds. Using the flux footprint parameterisation of Kljun et al. (2015), footprints were calculated for each averaging period using observed wind and stability conditions, and aggregated into 1 m s^{-1} wind speed bins. Using these aggregated footprints, the percentage of land area contribution in the footprint area was estimated to increase from 1–2% at high wind speeds to 15% at winds below 2 m s^{-1} (Figure 6). It should be noted that the footprint model is designed for flat homogeneous terrain – not a heterogeneous coastal site. For instance, land influence may be higher than estimated at low wind speeds as a consequence of the elevation of the headland relative to sea level.

Measured roughness lengths (z_0), calculated using Eq. (2–5), were also elevated at low wind speeds (Figure 7).

https://doi.org/10.5194/amt-2020-65
Preprint. Discussion started: 27 May 2020


Atmospheric Measurement Techniques Discussions

$$z_0 = z/e^{\left(\frac{kU}{u_*}-\Psi_m\left(\frac{z}{L}\right)\right)} \quad (2)$$

Where z_0 is roughness length in m, z is measurement height in m, κ is the von Kármán constant, U is wind speed in m s^{-1}, u_* is friction velocity in m s^{-1}, and $\Psi_m\left(\frac{z}{L}\right)$ is the integral of the universal function, defined as (Businger et al., 1971; Högström, 1988):

$$\Psi_m\left(\frac{z}{L}\right) = -6\frac{z}{L} \quad for\ \frac{z}{L} \geq 0 \quad (3)$$

$$\Psi_m\left(\frac{z}{L}\right) = ln\left[\left(\frac{1+x^2}{2}\right)\left(\frac{1+x}{2}\right)^2\right] - 2tan^{-1}x + \frac{\pi}{2} \quad for\ \frac{z}{L} < 0 \quad (4)$$

where

$$x = \left(1 - 19.3\frac{z}{L}\right)^{1/4} \quad (5)$$

Roughness lengths at high wind speeds are scattered approximately around 0.0002 m, which is expected for an open sea fetch (World Meteorological Organisation, 2008), but a large increase can be seen at wind speeds < 3 m s^{-1}. The increase is indicative of a surface with more roughness elements, such as the rocks and grass found on the headland. Inaccuracies in the double rotation method at low wind speeds can mean that the removal off horizontal wind from the rotated vertical component is incomplete, further contributing to the elevated surface values. This indicates the need for a filter to exclude land-influenced flux data. A wind speed filter of > 3 m s^{-1} was used in this work, though filters on the basis of z_0 could also be used to similar effect. While it could further decrease the possibility of land influence, a more stringent filter has not been applied to avoid excessive data removal.

Previous eddy covariance work on CO_2 has applied filters on the basis of friction velocity (u_*)(e.g. Barr et al., (2013)) to avoid underestimation of flux during periods of poorly developed turbulence, especially at night (Aubinet, 2008). However past measurements of oceanic ozone deposition have not reported using such a filter (Gallagher et al., 2001; Helmig et al., 2012; McVeigh et al., 2010), likely because very low wind speeds and u_* are uncommon over the ocean. For our data, removing data with u_* < 0.15 cm s^{-1} made no difference to the observed median deposition velocity. Therefore, given that a wind speed filter was already applied, no friction velocity filter was included.

Longer averaging periods than 20-minutes were also considered, but 60-minute averaging caused a large loss of data to the selection criteria. Missing data, as well as stationarity of wind and ozone especially contributed to an overall 23% reduction in total data accepted compared with 20-minute averaging. This shorter averaging time was therefore used to avoid loss of data to stationarity requirements while still observing reasonable lag times and cospectral shape.

5 Results

5.1 Flux and deposition values

https://doi.org/10.5194/amt-2020-65
Preprint. Discussion started: 27 May 2020


Atmospheric Measurement Techniques Discussions

From April 10th to May 21st, 2018, the median deposition velocity was 0.037 cm s^{-1} (interquartile range 0.017–0.063 cm s^{-1}) with a median mass flux of -0.132 mg m^{-2} h^{-1} and a median ozone concentration of 48 ppbv (Figure 8). The resulting distribution of v_d values was compared to that obtained with the lag time set to 180s, and was determined by a Kolmogorov-Smirnov test to be significantly different from the results of the disjoined data (Figure 10), rejecting the null hypothesis that the two sets of values could be taken by chance from the same distribution. 1σ flux uncertainty was determined for each 20-minute period (see Sect. 5.4), with a median uncertainty of 0.113 mg m^{-2} h^{-1}, corresponding to a deposition velocity uncertainty of 0.031 cm s^{-1}. This uncertainty reduces with the square root of the sample size where aggregated results are presented.

Previous eddy covariance ozone deposition velocity measurements have yielded values of 0.009–0.034 cm s^{-1} over five open ocean cruises (Helmig et al., 2012) with higher values typically corresponding to warmer oceans. Additionally, tower-based measurements have reported deposition at coastal locations to be 0.025 cm s^{-1} (McVeigh et al., 2010), 0.030 cm s^{-1} (Whitehead et al., 2009) and 0.13 cm s^{-1} (Gallagher et al., 2001). These measurements were carried out at Mace Head (west Ireland), Weybourne (east UK) and Roscoff (north-west France) respectively. Our median v_d of 0.037 cm s^{-1} is towards the upper end of previous work, though much lower than Gallagher et al. (2001).

5.2 Wind Speed Dependence

The dependence of v_d on wind speed and friction velocity (u_*) is examined in Figure 11A and B. Individual values that passed the filtering criteria exhibit a large degree of scatter, and are therefore presented alongside median values within wind speed bins of 1 m s^{-1} and friction velocity bins of 0.05 m s^{-1}. Note that v_d values removed by the wind speed filter (Sect. 4) are shown in the shaded region of Figure 11A to demonstrate the increase of v_d at low wind speeds, but are excluded from Figure 11B. Outside of the excluded low wind speed region, v_d values are relatively constant up to 10 m s^{-1}. Above 10 m s^{-1}, v_d begins to increase, though data are sparse above 14 m s^{-1}.

The wind speed dependency of v_d has been discussed in a number of other studies. Chang et al. (2004) report a five-fold increase in v_d (0.0158–0.0775 cm s^{-1}) from 0 to 20 m s^{-1}, with v_d near constant below 4 m s^{-1}, and approximately doubling from 4–10 m s^{-1}. Tower-based eddy covariance measurements by Gallagher et al. (2001) exhibit increasing ozone deposition as wind speed increases, with v_d tripling over the range u_* = 0.05–0.5 m s^{-1}. Using the same type of instrument, McVeigh et al. (2010) report a similar trend, fitting an exponential curve to their data. Lastly, deposition during two of the five cruises reported by Helmig et al. (2012) increases with increasing wind speeds. These data fit reasonably well to the parameterisation of Fairall et al. (2007):

$$v_d \cong \alpha\sqrt{AD_c} + \frac{\alpha}{6}\kappa u_{*w} \quad (6)$$

where α is the dimensionless solubility of ozone in water, A is the effective rate constant for the reaction of ozone with molecules in the surface water in s^{-1}, D_c is the molecular diffusion coefficient of ozone in water in m^2 s^{-1}, κ is the von

https://doi.org/10.5194/amt-2020-65
Preprint. Discussion started: 27 May 2020


Atmospheric Measurement Techniques Discussions

Kármán constant (0.4), and u_{*w} is the water-side friction velocity in m s^{-1}. The fit shown in blue in Figure 11B was determined using the relevant parameters during the experiment at the PPAO, with u_{*w} derived from u_* using:

$$u_{*w} = \sqrt{\frac{\rho_{air}}{\rho_{water}}} u_* \quad (7)$$

where ρ_{air} and ρ_{water} are the densities of air and water respectively. α, A, and D_c were determined empirically according to Eq. (8) (Morris, 1988), Eq. (9) (Magi et al., 1997), and Eq. (10) (Johnson and Davis, 1996):

$$\alpha = 10^{-0.25-0.013(T_s-273.16)} \quad (8)$$

$$A = [I^-] e^{\left(\frac{-8772.2}{T_s}+51.5\right)} \quad (9)$$

$$D_c = 1.1 \times 10^6 e^{\left(\frac{-1896}{T_s}\right)} \quad (10)$$

where T_s is the sea surface temperature (in K) and $[I^-]$ is the aqueous iodide concentration in mol dm^{-3}. We note that Eq. (9) only accounts for the reactivity of ozone with iodide in the sea surface. Other species present in the SML have also been shown to react with ozone (Martino et al., 2009; Shaw and Carpenter, 2013), but given the uncertainty surrounding their rate constants and any temperature dependence, they have been omitted here. Fixed T_s (284 K) and $[I^-]$ (85 nmol dm^{-3}) values from the relevant period and representative of the footprint of PPAO (Sherwen et al., 2019) were used to determine α, A, and D_c, and thus v_d (cm s^{-1}) using Eq. (6) (shown in blue on Figure 11B). This can be simplified to:

$$v_{d\ predicted} = 0.01324 + 0.09378 u_*$$

In comparison, the linear fit of our experimental 20-minute v_d values against u_* is:

$$v_{d\ measured} = 0.02017 + 0.07537 u_*$$

Our results therefore show comparable, but slightly lower dependence on friction velocity (and therefore also wind speed) than predicted by the parameterisation of Fairall et al. (2007). Given the assumptions of the simplified model (Eq. (6)) and the uncertainties in various parameters, not least the rate constant for the reaction of O_3 with I^- (e.g. Moreno & Baeza-Romero, 2019), this agreement is remarkable. The two-layer model of Luhar et al. (2018) for the same data is shown in black in Figure 11B. Considering only iodide reactivity, this model appears to under-predict deposition compared with the one-layer model of Fairall et al. (2007), and lacks any major dependence on wind speed except during very calm conditions (see Sect. 6 for further discussion).

5.3 Land and Tidal Influence

Footprint analysis of the PPAO site (as discussed in Sect. 4) suggests that the spatial contribution of land surfaces to our observed deposition is 3.9%. However, deposition to land is typically greater than to the ocean, amplifying the potential

https://doi.org/10.5194/amt-2020-65
Preprint. Discussion started: 27 May 2020


Atmospheric Measurement Techniques Discussions

influence on our data. If our observations were adjusted for 3.9% spatial contribution of grassland ($v_d \approx 0.25$ cm s^{-1}, Hardacre et al., 2015), then our calculated coastal water v_d would be 0.028 cm s^{-1} (23% lower than we measured). In reality the terrain is a mixture of grassland and rocky shoreline, varying in extent with the tide, so the land v_d discussed above may be an overestimate. Although there are insufficient data over the land to the north-west to reliably determine a v_d value for the land around the PPAO, an estimate can be made by obtaining a least square solution using the land cover determined in Figure 6 and the observed v_d values in Figure 11A. Data from wind speeds > 14 m s^{-1} were not used (only 4 data points). Using all data from 2–13 m s^{-1} yielded values of 0.167 cm s^{-1} and 0.034 cm s^{-1} for land and sea respectively, suggesting a lesser effect from land than using the fixed value from Hardacre et al. (2015). Given that the land contribution in Figure 6 doesn't stabilise until 9 m s^{-1}, it is possible that constant v_d between 4 and 10 m s^{-1} wind speeds (Figure 11A) may be a consequence of land influence and wind speed enhancement counteracting one another. Estimated water-only v_d values, calculated by subtracting the product of the land fraction and the land v_d value from the measured v_d, are shown in Figure 13.

It is worth reiterating that this footprint model is designed for use in homogenous environments, which is not true of our site. Furthermore, the double rotation applied to the wind data will result in varying pitch angles relative to the water surface, introducing a dependence of the footprint extent on this pitch angle. These limitations may be important for work relying on direct interpretations of the flux footprint, such as comparisons to emissions inventories (Squires et al., 2020; Vaughan et al., 2017). In contrast, we use aggregates of these individual footprints only to develop a strategy for robust data selection.

The PPAO site flux footprint also experiences periodic variations associated with the tide, which alters the effective measurement height and changes the land type in the footprint when the shoreline is exposed. Whitehead et al. (2009) provide an extreme example of this, reporting v_d increasing from 0.030 cm s^{-1} at high tide to 0.21 cm s^{-1} at low tide during the day at a site with a tidal range of 9 m. The tide also causes periodic movement of the river plume around the Penlee headland, altering the salinity and composition of the surface water (Yang et al., 2016).

Measurement height was adjusted for tide height using tidal data from the British Oceanographic Data Centre (BODC), measured approximately 6 km upstream. Periodograms were also used to look for periodic deposition variation from exposed shoreline or riverine water, but none could be identified above the variability in the data. Gallagher et al. (2001) report a tentative (though statistically insignificant) diurnal cycle for coastal water during observations made at Weybourne in East Anglia, UK. However, no such trend was observed in the PPAO flux data.

5.4 Measurement uncertainty

To understand the variability in our v_d observations, a flux limit of detection was obtained empirically according to the method of Langford et al. (2015). For each averaging period, cross-correlation functions (discussed in Sect. 3) were calculated at a series of improbable lag times (150–180 seconds), and the root mean squared deviation of these values was taken to be representative of the random error of the flux measurement. Limits of detection were calculated for each averaging period due to its dependence on wind speed and atmospheric stability, giving a median 2σ flux limit of detection

https://doi.org/10.5194/amt-2020-65
Preprint. Discussion started: 27 May 2020


Atmospheric Measurement Techniques Discussions

of 0.113 mg m^{-2} h^{-1}. At the average ozone concentration of 48 ppbv, this equates to a deposition velocity of 0.033 cm s^{-1}, with 305 of the 491 averaging periods exceeding their individually determined 2σ limit of detection.

Alternatively, a theoretical estimation of flux uncertainty can be made according to the expression given by Fairall et al. (2000):

$$\Delta F_\chi = \Delta\overline{w'X'} \approx \frac{\sigma_w \sigma_X}{\sqrt{T/\tau_{wca}}} \quad (11)$$

where ΔF_X is flux uncertainty, w' is instantaneous vertical wind velocity fluctuation, X' is instantaneous ozone fluctuation, σ_w is the standard deviation in vertical wind velocity, σ_X is the standard deviation in ozone concentration, T is length of the averaging period in seconds, and τ_{wca} is the integral timescale for vertical fluctuations. A factor with a value of 1–2 is sometimes also included to reflect uncertainty in this relationship (Blomquist et al., 2010). The integral timescale τ_{wca} can either be determined from a flux cospectrum peak frequency:

$$\tau_{wca} = \frac{1}{2\pi f_{max}} \quad (12)$$

or empirically according to:

$$\tau_{wca} = \frac{az}{U} \quad (13)$$

where z is measurement height in meters, U is mean wind speed, and a is a value that varies with atmospheric stability. The value of a has been reported variably as 0.3–3 for near neutral conditions (Blomquist et al., 2010; Lenschow and Kristensen, 1985) and on the order of 10–12 for convective/unstable conditions (Blomquist et al., 2010; Fairall, 1984). Using the peak frequency of the cospectrum shown in Figure 14 (0.07 Hz), τ_{wca} was determined to be approximately 2.2 s during near-neutral conditions and wind speeds of 12.1 m s^{-1}. This corresponds to a value for a of 1.5, similar to the literature. Since individual 20-minute cospectra were too noisy, this a value was used with Eq. (13) to determine τ_{wca} for each 20-minute period. It should be noted that the value of a is stability dependent. However, since stability was near neutral for most periods (z/L = -0.39 to 0.15, 20th–80th percentile), the effects of varying stability on a are expected to be small.

Using these integral timescales, a theoretical flux uncertainty can be calculated for each averaging period using Eq. (11). The theoretical values obtained were much higher than those found empirically – the median theoretical 2σ limit of detection was 0.241 mg m^{-2} h^{-1}. We note however that this is an approximation, derived from the work of Lenschow & Kristensen (1985) who defined twice the right-hand side of Eq. (11) to be an upper limit on flux uncertainty.

Equation (11) demonstrates how the variability of ozone and vertical wind are directly related to uncertainty in the measured flux. White noise in the wind measurement is expected to be very small, such that random instrument noise likely represents a significant contribution to the total variance of ozone observed at 10 Hz. Given the relatively low sensitivity of the instrument used in this work (240 counts ppbv $^{-1}$ s^{-1} compared to 2800 counts ppbv^{-1} s^{-1} reported by Helmig et al. (2012)), autocovariances were calculated for each averaging period using the 10 Hz ozone data to examine the extent to which variance in ozone concentration is caused by instrument white noise. White noise only correlates with itself at zero lag time,

https://doi.org/10.5194/amt-2020-65
Preprint. Discussion started: 27 May 2020


Atmospheric Measurement Techniques Discussions

so it can be estimated from the difference between the first and second points in an autocovariance plot (Blomquist et al., 2010). Instrument white noise derived using this approach was found to contribute 45–98% to the total ozone variance (10^{th}–90^{th} percentile), with a median σ_{noise} of 1.4 ppbv. A more sensitive ozone instrument could therefore significantly improve the flux uncertainty at a 20-minute averaging period.

Besides the random uncertainty discussed above, systematic errors are also worthy of some consideration. Specifically, whether the highest and lowest frequencies of turbulence have been adequately observed. High frequency information can be lost if measurements are made too infrequently, or if the sample is attenuated significantly in the sample line. Measurements at 10 Hz, as performed here, are widely considered sufficient to observe this high frequency structure. Laminar flow was also avoided through the length of the sample line (Reynolds number = 3000). As a result, the cospectrum in Figure 14 shows no major loss of high frequency information compared to theory. Since fluxes were calculated over 20-minute averaging periods using linear detrending, there is also a chance that low frequency information may not be fully observed. Firstly, using a simple block average in place of linear detrending had little effect on the median flux observed (+1.7%). Using an averaging period of 1 hour instead of 20 minutes gave slightly larger magnitude flux (+4.1%) as well. However, the longer period lead to much greater data loss (22%) to the selection criteria in Sect. 4, hence the 20-minute average was used for this work. This suggests that any low frequency loss is approximately 5% the total flux – a small amount relative to the calculated random uncertainty.

6 Discussion

For the average meteorological conditions observed during this work, the one-layer model of Fairall et al. (2007) predicts a deposition of 0.037 cm s^{-1}. Here, one-layer refers to considering the surface water to have uniform reactivity to ozone with depth, rather than a thin sublayer at the surface where reactivity is enhanced (a two-layer model). By contrast, the revised 2-layer model of Luhar et al. (2018) predicts a deposition of 0.016 cm $^{-1}$ for the same conditions using a fixed reaction-diffusion sublayer (δ_m) of 3 μm. An iodide concentration of ~600 nmol dm^{-3} would be necessary to yield the observed deposition – much higher than a typical oceanic value of 77 nmol dm^{-3} (Chance et al., 2014). However, DOM (Shaw and Carpenter, 2013), chlorophyll (Clifford et al., 2008) and surfactants (McKay et al., 1992) have also been shown to enhance ozone deposition. Therefore the effective pseudo-first order rate constant for the reaction of ozone with water, A, is likely to be significantly higher than accounted for by iodide alone in Eq. (9). Chang et al. (2004) defined this total reactivity as:

$$A = \sum_i k_i C_i \quad (14)$$

Where A is the effective pseudo-first order rate constant for the reaction of ozone with water, k_i and C_i are the second order rate constant and concentration of species i respectively. We can therefore include an estimate of the effects of DOM reactivity using a typical oceanic DOM concentration of 52 μmol dm^{-3} (Massicotte et al., 2017) and a rate constant of 3.7×10^{-6} dm^3 mol^{-1} s^{-1} (average of the values reported by Sarwar et al. (2016) and Coleman et al. (2010)). Doing so increases A

https://doi.org/10.5194/amt-2020-65
Preprint. Discussion started: 27 May 2020


Atmospheric Measurement Techniques Discussions

from 544 s^{-1} to 737 s^{-1} and leads to increased deposition values of 0.048 cm s^{-1} and 0.028 cm s^{-1} for the models of Fairall and Luhar, respectively.

The magnitude of the effect of DOM on O_3 deposition remains highly uncertain due to the uncertainties in how O_3 interacts with DOM and surfactants, variability in the sea-surface microlayer (SML) composition, and the effect of temperature. The coastal waters near the PPAO experience large phytoplankton growth during the 'spring bloom' (Cushing, 1959; Smayda, 1998), and the organic content and composition of the SML could be very different compared to the open ocean. The seasonal and spatial variations in these O_3-reactive substances could, in turn drive differences in ozone deposition. For example, Bariteau et al. (2010) reported v_d increasing from 0.034 cm s^{-1} to 0.065 cm s^{-1} as the waters changed from open ocean into coastal during the TexAQS-2006 cruise. It is unclear how much of the observed gradient is a result of SML composition or of terrestrial influence. Similarly, Ganzeveld et al. (2009) encountered underestimation of coastal ozone deposition in their modelling work when DOM reactivity was omitted, suggesting that this may be a particularly important factor in coastal environments. While the model of Fairall et al. (2007) appears to match our observed v_d well, it is possible that this is a consequence of some missing reactivity. Inclusion of DOM causes the one-layer model to overestimate v_d, as reported by Luhar et al. (2018).

If the two-layer model provides more accurate deposition velocities with adequate reactivity information, then it shows little dependence upon wind speed in all but the calmest conditions. This would stand in contrast to the one-layer model, and a number of experimental observations including those presented here.

7 Summary and conclusions

An ozone chemiluminescence detector adapted from an Eco Physics® CLD 886 NO_x detector was used to measure the ozone deposition velocity to the sea surface at a coastal site near Plymouth, on the southwest coast of the UK. The median observed deposition velocity was 0.037 cm s^{-1}, comparable with past work, but at the upper end of the values obtained by Helmig et al. (2012) during ship-based, open-ocean measurements (0.009–0.034 cm^{-1}).

Using observed meteorology with the model of Luhar et al. (2018) yields a predicted v_d of 0.018 cm s^{-1} in the absence of DOM reactivity, or 0.026 cm s^{-1} with estimated DOM concentration of 52 µmol dm^{-3} and a O_3 + DOM rate constant of 3.7×10^{-6} dm^3 mol^{-1} s^{-1}. We suspect that the difference from our measured v_d is due to the uncertainty surrounding the reaction between O_3 and DOM, and the timing of our measurements, which coincide with the spring bloom and potential enhancements in surface microlayer reactive organics.

Elevated deposition was observed at low wind speeds, contrary to predictions (Chang et al., 2004) and to previous observations (Helmig et al., 2012). We attribute this observation to a contribution to v_d from land within the footprint during periods of low wind. Periods with wind speeds > 3 m s^{-1} (corresponding to approximately < 10% land cover in the footprint) were used to evaluate v_d. However, the possibility of land influence could not be completely removed, with our oceanic v_d estimates potentially overestimated by 8%, even after wind speed filtering. Deposition velocity showed a linear dependence

https://doi.org/10.5194/amt-2020-65
Preprint. Discussion started: 27 May 2020


Atmospheric Measurement Techniques Discussions

on friction velocity comparable to that predicted by the parameterisation of Fairall et al. (2007), though with considerable scatter. The potential for tidal effects on v_d (exposing shoreline and input of river water with different chemical composition) were also examined, though no clear periodicity could be observed, either at the tidal frequency or on a diurnal timescale. Cross-covariance was used to empirically determine a 2σ limit of detection for each averaging period. This limit of detection was exceeded in 305 out of 491 periods. Auto-covariance of high-frequency ozone data indicated that instrument noise was a significant component in the observed ozone variability, and lowering the noise level would reduce the flux uncertainty. Future work will link the properties of the sea-surface microlayer in the footprint area to observed O_3 fluxes. A larger dataset may help to elucidate the influence of biogeochemical parameters, seasonal variation and wind speed dependence, which have not been definitively characterised to date.

Code and data availability: the eddy4R software packages used in these analyses are maintained at https://github.com/NEONScience/NEON-FIU-algorithm. 20-minute data have been submitted to the Centre for Environmental Data Analysis (CEDA), awaiting DOI. The corresponding author can be contacted directly for the full high-frequency data.

Author contribution: Experimental work was carried out by DCL, TGB and MY. DCL also conducted the formal analysis and visualisation of the results, with relevant supervision from TGB and MY. SM developed the eddy4R codebase, with ARV providing modification for its use here. RJP provided software for instrumentation and validation of model applications to the data. JDL and LJC supervised the interpretation of the results. The work was proposed by LJC, who also acquired the necessary funding. DCL Prepared the manuscript with all authors contributing to the editing process.

Competing interests: The authors declare that they have no conflict of interest.

8 Acknowledgements

LJC and DCL thank funding from the Natural Environment Research Council (NERC), UK, through the grant "Iodide in the ocean: distribution and impact on iodine flux and ozone loss" (NE/N009983/1). DCL also thanks NERC for the funding of his PhD project (NERC SPHERES DTP NE/L002574/1). LJC acknowledges funding from the European Research Council (ERC) under the European Union's horizon 2020 programme (Grant agreement No. 833290). Trinity House (https://www.trinityhouse.co.uk/, accessed 10/1/20) owns the Penlee Point Atmospheric Observatory (PPAO) site, who allow Plymouth Marine Laboratory (PML) use the building to house instrumentation. Access to the site is arranged thanks to Mount Edgcumbe Estate (https://www.mountedgcumbe.gov.uk/, accessed 10/1/20). PPAO research (including the contributions of T.G.B. and M.Y. to this manuscript) is supported by NERC via the national capability ACSIS project (grant no. NE/N018044/1). We thank Frances Hopkins (PML), Daniel Philips (University of East Anglia) and Oban Jones (PML) for assistance at the field site. This work is contribution number 8 from the PPAO. The National Ecological Observatory Network is a project sponsored by the National Science Foundation and managed under co-operative agreement by Battelle. This material is based upon work supported by the National Science Foundation (Grant DBI-0752017). Any opinions,

https://doi.org/10.5194/amt-2020-65
Preprint. Discussion started: 27 May 2020


Atmospheric Measurement Techniques Discussions

findings, and conclusions or recommendations expressed in this material are those of the author and do not necessarily reflect the views of the National Science Foundation.

References

Aldaz, L.: Flux Measurements of Atmospheric Ozone Over Land Water, J. Geophys. Res., 74(28), 6943–6946, 1969.

Aubinet, M.: Eddy Covariance CO2 Flux Measurements in Nocturnal Conditions: an Analysis of the Problem, Ecol. Appl., 18(6), 1368–1378, 2008.

Bariteau, L., Helmig, D., Fairall, C. W., Hare, J. E., Hueber, J. and Lang, E. K.: Determination of oceanic ozone deposition by ship-borne eddy covariance flux measurements, Atmos. Meas. Tech., 3(2), 441–455, doi:10.5194/amt-3-441-2010, 2010.

Barr, A. G., Richardson, A. D., Hollinger, D. Y., Papale, D., Arain, M. A., Black, T. A., Bohrer, G., Dragoni, D., Fischer, M. L., Gu, L., Law, B. E., Margolis, H. A., Mccaughey, J. H., Munger, J. W., Oechel, W. and Schaeffer, K.: Use of change-point detection for friction-velocity threshold evaluation in eddy-covariance studies, Agric. For. Meteorol., 171–172, 31–45, doi:10.1016/j.agrformet.2012.11.023, 2013.

Blomquist, B. W., Huebert, B. J., Fairall, C. W. and Faloona, I. C.: Determining the sea-air flux of dimethylsulfide by eddy correlation using mass spectrometry, Atmos. Meas. Tech., 3(1), 1–20, doi:10.5194/amt-3-1-2010, 2010.

Brock, F. V.: A Nonlinear Filter to Remove Impulse Noise from Meteorological Data, J. Atmos. Ocean. Technol., 3(1), 51–58, doi:10.1175/1520-0426(1986)003<0051:anftri>2.0.co;2, 1986.

Businger, J. A., Wyngaard, J. C., Izumi, Y. and Bradley, E. F.: Flux- profile relationships in the atmospheric surface layer, J. Atmos. Sci., 28(2), 181–189, 1971.

Chance, R., Baker, A. R., Carpenter, L. and Jickells, T. D.: The distribution of iodide at the sea surface., Environ. Sci. Process. Impacts, 16, 1841–1859, doi:10.1039/c4em00139g, 2014.

Chang, W., Heikes, B. G. and Lee, M.: Ozone deposition to the sea surface: Chemical enhancement and wind speed dependence, Atmos. Environ., 38(7), 1053–1059, doi:10.1016/j.atmosenv.2003.10.050, 2004.

Clifford, D., Donaldson, D. J., Brigante, M., D'Anna, B. and George, C.: Reactive uptake of ozone by chlorophyll at aqueous surfaces, Environ. Sci. Technol., 42(4), 1138–1143, doi:10.1021/es0718220, 2008.

Coleman, L., Varghese, S., Tripathi, O. P., Jennings, S. G. and O'Dowd, C. D.: Regional-Scale Ozone Deposition to North-East Atlantic Waters, Adv. Meteorol., 2010, 1–16, doi:10.1155/2010/243701, 2010.

Cushing, D. H.: The seasonal variation in oceanic production as a problem in population dynamics, ICES J. Mar. Sci., 24(3), 455–464, doi:10.1093/icesjms/24.3.455, 1959.

Fairall, C. W.: Interpretation of eddy-correlation measurements of particulate deposition and aerosol flux, Atmos. Environ., 18(7), 1329–1337, 1984.

Fairall, C. W., Hare, J. E., Edson, J. B. and McGillis, W.: Parameterization and Micrometeorological Measurement of Air-Sea Gas Transfer., 2000.

Fairall, C. W., Helmig, D., Ganzeveld, L., Hare, J. and Science, E.: Water-side turbulence enhancement of ozone deposition to the ocean, Atmos. Chem. Phys., 443-451 ST-Water-side turbulence enhancement of, 2007.

Foken, T.: Micrometeorology, 1st ed., Springer-Verlag Berlin Heidelberg., 2008.

Galbally, I. E. and Roy, C. R.: Destruction of ozone at the earth's surface, Q. J. R. Meteorol. Soc., 106(449), 599–620,

doi:10.1002/qj.49710644915, 1980.

Gallagher, M. W., Beswick, K. M. and Coe, H.: Ozone deposition to coastal waters, Q. J. R. Meteorol. Soc., 127(October 1999), 539–558, doi:10.1002/qj.49712757215, 2001.

Ganzeveld, L., Helmig, D., Fairall, C. W., Hare, J. and Pozzer, A.: Atmosphere-ocean ozone exchange: A global modeling study of biogeochemical, atmospheric, and waterside turbulence dependencies, Global Biogeochem. Cycles, 23(4), 1–16, doi:10.1029/2008GB003301, 2009.

Garland, J. A., Elzerman, A. W., Penkett, A. A.: The mechanism for dry deposition of ozone to seawater surface, J. Geophys. Res., 85, 7488–7492, 1980.

Hardacre, C., Wild, O. and Emberson, L.: An evaluation of ozone dry deposition in global scale chemistry climate models, Atmos. Chem. Phys., 15(11), 6419–6436, doi:10.5194/acp-15-6419-2015, 2015.

Heck, W. W., Taylor, O. C., Adams, R., Bingham, G., Miller, J., Preston, E. and Weinstein, L.: Assessment of Crop Loss from Ozone, J. Air Pollut. Control Assoc., 32(4), 353–361, doi:10.1080/00022470.1982.10465408, 1982.

Helmig, D., Lang, E. K., Bariteau, L., Boylan, P., Fairall, C. W., Ganzeveld, L., Hare, J. E., Hueber, J. and Pallandt, M.: Atmosphere-ocean ozone fluxes during the TexAQS 2006, STRATUS 2006, GOMECC 2007, GasEx 2008, and AMMA 2008 cruises, J. Geophys. Res. Atmos., 117(4), 1–15, doi:10.1029/2011JD015955, 2012.

Högström, U.: Non-dimensional wind and temperature profiles in the atmospheric surface layer: A re-evaluation, Boundary-Layer Meteorol., 42(1–2), 55–78, doi:10.1007/BF00119875, 1988.

Johnson, P. N. and Davis, R. A.: Diffusivity of ozone in water, J. Chem. Eng. Data, 41(6), 1485–1487, doi:10.1021/je9602125, 1996.

Kawa, S. R. and Pearson, R.: Ozone budgets from the dynamics and chemistry of marine stratocumulus experiment, J. Geophys. Res., 94(D7), 9809, doi:10.1029/jd094id07p09809, 1989.

Kljun, N., Calanca, P., Rotach, M. W. and Schmid, H. P.: A simple two-dimensional parameterisation for Flux Footprint Prediction (FFP), Geosci. Model Dev., 8(11), 3695–3713, doi:10.5194/gmd-8-3695-2015, 2015.

Langford, B., Acton, W., Ammann, C., Valach, A. and Nemitz, E.: Eddy-covariance data with low signal-to-noise ratio: Time-lag determination, uncertainties and limit of detection, Atmos. Meas. Tech., 8(10), 4197–4213, doi:10.5194/amt-8-4197-2015, 2015.

Lelieveld, J. and Dentener, F. J.: What controls tropospheric ozone?, J. Geophys. Res., 105(1999), 3531, doi:10.1029/1999JD901011, 2000.

Lenschow, D. H. and Kristensen, L.: Uncorrelated noise in turbulence measurements, J. Atmos. Ocean. Technol., 2(1), 68–81, doi:10.1175/1520-0426(1985)002<0068:UNITM>2.0.CO;2, 1985.

Lenschow, D. H., Pearson, R. and Stankov, B. B.: Measurements of ozone vertical flux to ocean and forest, J. Geophys. Res. Ocean., 87(C11), 8833–8837, doi:10.1029/JC087iC11p08833, 1982.

Luhar, A. K., Woodhouse, M. T. and Galbally, I. E.: A revised global ozone dry deposition estimate based on a new two-layer parameterisation for air-sea exchange and the multi-year MACC composition reanalysis, Atmos. Chem. Phys., 18(6), 4329–4348, doi:10.5194/acp-18-4329-2018, 2018.

Macdonald, S. M., Gómez Martín, J. C., Chance, R., Warriner, S., Saiz-Lopez, A., Carpenter, L. J. and Plane, J. M. C.: A laboratory characterisation of inorganic iodine emissions from the sea surface: Dependence on oceanic variables and parameterisation for global modelling, Atmos. Chem. Phys., 14(11), 5841–5852, doi:10.5194/acp-14-5841-2014, 2014.

Magi, L., Schweitzer, F., Pallares, C., Cherif, S., Mirabel, P. and George, C.: Investigation of the Uptake Rate of Ozone and Methyl Hydroperoxide by Water Surfaces, J. Phys. Chem. A, 101(27), 4943–4949, doi:10.1021/jp970646m, 1997.

Martino, M., Mills, G. P., Woeltjen, J. and Liss, P. S.: A new source of volatile organoiodine compounds in surface seawater, Geophys.

Res. Lett., 36(1), 2–6, doi:10.1029/2008GL036334, 2009.

Martino, M., Lézé, B., Baker, A. R. and Liss, P. S.: Chemical controls on ozone deposition to water, Geophys. Res. Lett., 39(5), 39–43, doi:10.1029/2011GL050282, 2012.

Massicotte, P., Asmala, E., Stedmon, C. and Markager, S.: Global distribution of dissolved organic matter along the aquatic continuum: Across rivers, lakes and oceans, Sci. Total Environ., 609, 180–191, doi:10.1016/j.scitotenv.2017.07.076, 2017.

McKay, W. A., Stephens, B. A. and Dollard, G. J.: Laboratory Measurements of Ozone Deposition To Sea-Water and Other Saline Solutions, Atmos. Environ. Part a-General Top., 26(17), 3105–3110, 1992.

McVeigh, P., O'Dowd, C. and Berresheim, H.: Eddy Correlation Measurements of Ozone Fluxes over Coastal Waters West of Ireland, Adv. Meteorol., 2010, 1–7, doi:10.1155/2010/754941, 2010.

Medina-Ramón, M., Zanobetti, A. and Schwartz, J.: The effect of ozone and PM10 on hospital admissions for pneumonia and chronic obstructive pulmonary disease: A national multicity study, Am. J. Epidemiol., 163(6), 579–588, doi:10.1093/aje/kwj078, 2006.

Metzger, S., Durden, D., Sturtevant, C., Luo, H., Pingintha-Durden, N., Sachs, T., Serafimovich, A., Hartmann, J., Li, J., Xu, K. and Desai, A. R.: Eddy4R 0.2.0: A DevOps model for community-extensible processing and analysis of eddy-covariance data based on R, Git, Docker, and HDF5, Geosci. Model Dev., 10(9), 3189–3206, doi:10.5194/gmd-10-3189-2017, 2017.

Moreno, C. and Baeza-Romero, M. T.: A kinetic model for ozone uptake by solutions and aqueous particles containing I − and Br − , including seawater and sea-salt aerosol , Phys. Chem. Chem. Phys., 19, doi:10.1039/c9cp03430g, 2019.

Morris, J. C.: The aqueous solubility of ozone - a review, Ozone News, 1, 14–16 [online] Available from: http://bmt-berlin.com/Lit-1_CMorris.pdf, 1988.

Pound, R. J., Sherwen, T., Helmig, D., Carpenter, L. J. and Evans, M. J.: Influences of oceanic ozone deposition on tropospheric photochemistry, Atmos. Chem. Phys. Discuss. [online] Available from: https://doi.org/10.5194/acp-2019-1043, 2019.

Sarwar, G., Kang, D., Foley, K., Schwede, D., Gantt, B. and Mathur, R.: Technical note: Examining ozone deposition over seawater, Atmos. Environ., 141, 255–262, doi:10.1016/j.atmosenv.2016.06.072, 2016.

Shaw, M. D. and Carpenter, L. J.: Modification of ozone deposition and I2 emissions at the air-aqueous interface by dissolved organic carbon of marine origin, Environ. Sci. Technol., 47(19), 10947–10954, doi:10.1021/es4011459, 2013.

Sherwen, T., Chance, R. J., Tinel, L., Ellis, D., Evans, M. J. and Carpenter, L. J.: A machine learning based global sea-surface iodide distribution, Earth Syst. Sci. Data Discuss., (March), 1–40, doi:10.5194/essd-2019-40, 2019.

Smayda, T. J.: Patterns of variability characterizing marine phytoplankton, with examples from Narragansett Bay, ICES J. Mar. Sci., 55(4), 562–573, doi:10.1006/jmsc.1998.0385, 1998.

Squires, F. A., Nemitz, E., Langford, B., Wild, O., Drysdale, W. S., Acton, W. J. F., Fu, P., Grimmond, C. S. B., Hamilton, J. F., Hewitt, C. N., Hollaway, M., Kotthaus, S., Lee, J., Metzger, S., Pingintha-durden, N., Shaw, M., Vaughan, A. R., Wang, X., Wu, R., Zhang, Q. and Zhang, Y.: Measurements of traffic dominated pollutant emissions in a Chinese megacity, Atmos. Chem. Phys. Discuss., (x), 1–33, 2020.

Starkenburg, D., Metzger, S., Fochesatto, G. J., Alfieri, J. G., Gens, R., Prakash, A. and Cristóbal, J.: Assessment of despiking methods for turbulence data in micrometeorology, J. Atmos. Ocean. Technol., 33(9), 2001–2013, doi:10.1175/JTECH-D-15-0154.1, 2016.

Stevenson, D. S., Young, P. J., Naik, V., Lamarque, J. F., Shindell, D. T., Voulgarakis, A., Skeie, R. B., Dalsoren, S. B., Myhre, G., Berntsen, T. K., Folberth, G. A., Rumbold, S. T., Collins, W. J., MacKenzie, I. A., Doherty, R. M., Zeng, G., Van Noije, T. P. C., Strunk, A., Bergmann, D., Cameron-Smith, P., Plummer, D. A., Strode, S. A., Horowitz, L., Lee, Y. H., Szopa, S., Sudo, K., Nagashima, T., Josse, B., Cionni, I., Righi, M., Eyring, V., Conley, A., Bowman, K. W., Wild, O. and Archibald, A.: Tropospheric ozone changes, radiative forcing and attribution to emissions in the Atmospheric Chemistry and Climate Model Intercomparison Project (ACCMIP), Atmos. Chem. Phys., 13(6), 3063–3085, doi:10.5194/acp-13-3063-2013, 2013.

https://doi.org/10.5194/amt-2020-65
Preprint. Discussion started: 27 May 2020

Atmospheric Measurement Techniques Discussions

Vaughan, A. R., Lee, J. D., Shaw, M. D., Misztal, P. K., Metzger, S., Vieno, M., Davison, B., Karl, T. G., Carpenter, L. J., Lewis, A. C., Purvis, R. M., Goldstein, A. H. and Hewitt, C. N.: VOC emission rates over London and South East England obtained by airborne eddy covariance, Faraday Discuss., 200, 599–620, doi:10.1039/c7fd00002b, 2017.

Webb, E. K., Pearman, G. I. and Leuning, R.: Correction of flux measurements for density effects due to heat and water vapour transfer, Q. J. R. Meteorol. Soc., 106, 85–100 [online] Available from: http://www3.interscience.wiley.com/journal/114056302/abstract, 1980.

Whitehead, J. D., Mcfiggans, G. B., Gallagher, M. W. and Flynn, M. J.: Direct linkage between tidally driven coastal ozone deposition fluxes, particle emission fluxes, and subsequent CCN formation, Geophys. Res. Lett., 36(4), 1–5, doi:10.1029/2008GL035969, 2009.

World Meteorological Organisation: Guide to meteorological instruments and methods of observation., 7th ed., WMO-No. 8., 2008.

Yang, M., Bell, T. G., Hopkins, F. E., Kitidis, V., Cazenave, P. W., Nightingale, P. D., Yelland, M. J., Pascal, R. W., Prytherch, J., Brooks, I. M. and Smyth, T. J.: Air-sea fluxes of CO2 and CH4 from the penlee point atmospheric observatory on the south-west coast of the UK, Atmos. Chem. Phys., 16(9), 5745–5761, doi:10.5194/acp-16-5745-2016, 2016a.

Yang, M., Bell, T. G., Hopkins, F. E. and Smyth, T. J.: Attribution of atmospheric sulfur dioxide over the English Channel to dimethyl sulfide and changing ship emissions, Atmos. Chem. Phys., 16(8), 4771–4783, doi:10.5194/acp-16-4771-2016, 2016b.

Yang, M., Bell, T. G., Brown, I. J., Fishwick, J. R., Kitidis, V., Nightingale, P. D., Rees, A. P. and Smyth, T. J.: Insights from year-long measurements of air-water CH4 and CO2 exchange in a coastal environment, Biogeosciences Discuss., 16, 961–978, doi:10.5194/bg-2018-503, 2019.

Zhou, X. and Mopper, K.: Photochemical production of low-molecular-weight carbonyl compounds in seawater and surface microlayer and their air-sea exchange, Mar. Chem., 56(3–4), 201–213, doi:10.1016/S0304-4203(96)00076-X, 1997.

Table 1: Selection criteria applied to calculated fluxes, with number (and percent) of points remaining.

Selection Criterion	Number of 20-minute periods (%)
Sufficient data in 180–240° wind sector	723 (100%)
Ozone stationarity (trend < 6 ppbv)	689 (95.3%)
Wind stationarity (σ_{wd}) < 10°	630 (87.1%)
Ozone variability σ_{O3} < 2 ppbv	559 (77.3%)
Sensitivity within 3σ of mean	547 (75.7%)
Wind speed > 3 m s^{-1}	491 (67.9%)

https://doi.org/10.5194/amt-2020-65
Preprint. Discussion started: 27 May 2020

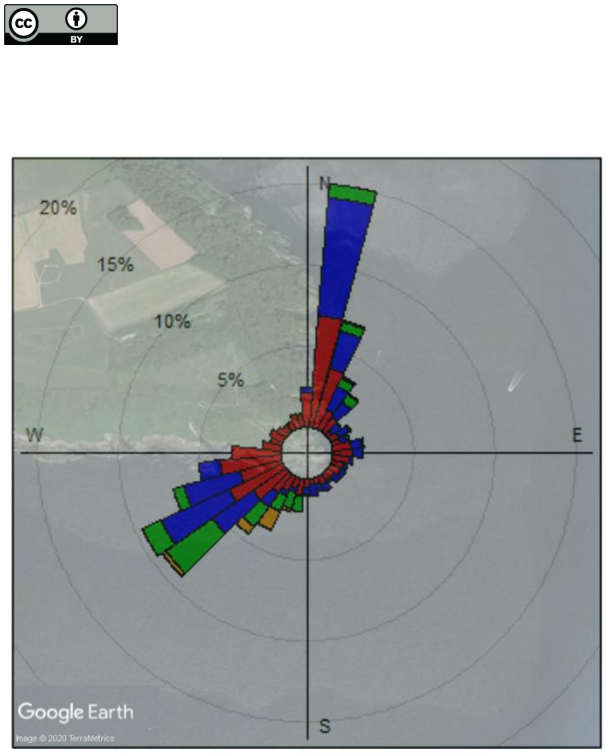

Figure 1: Wind directions and speeds at the PPAO during the study period. Radial percentage values indicate the portion of all observed wind that fell within a given sector. © Google Earth.

https://doi.org/10.5194/amt-2020-65
Preprint. Discussion started: 27 May 2020

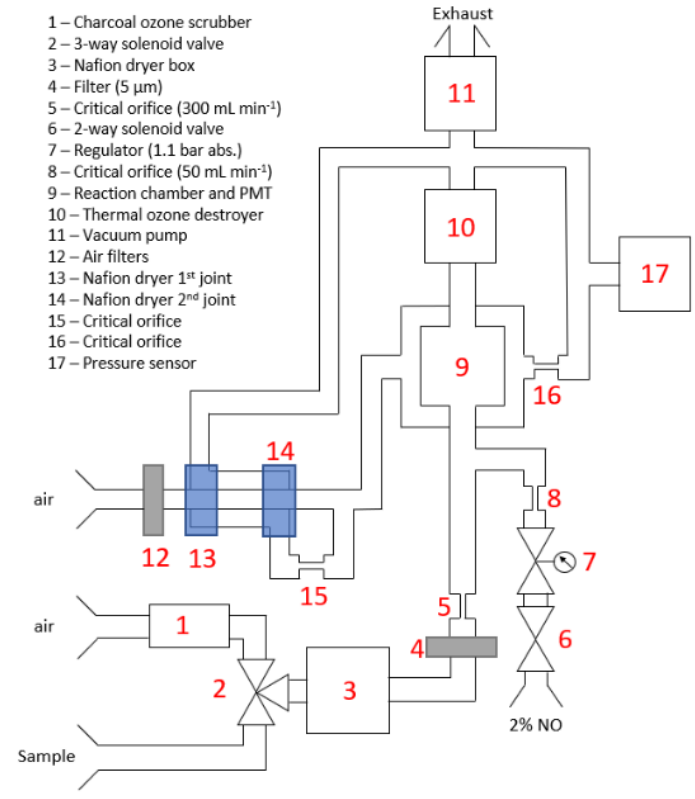

Figure 2: Schematic of the ozone chemiluminescence detector.

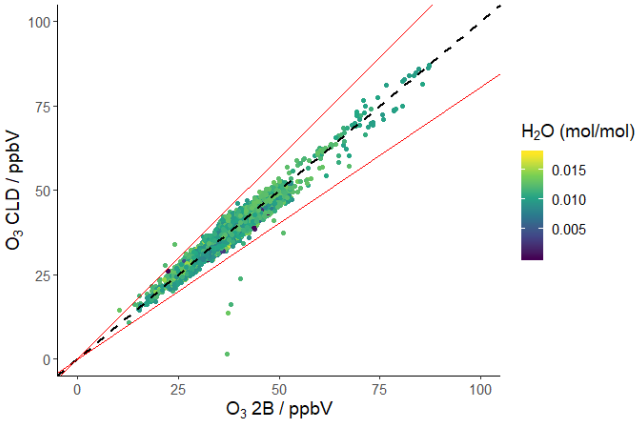

Figure 3: Comparison of 2B and CLD measured ozone concentration using a fixed sensitivity for the CLD of 240 counts ppbv^{-1} s^{-1}. The dotted line is x = y, and the red lines indicate a 3σ deviation from mean sensitivity, used in data filtering. Colour bar indicates the water vapour mixing ratio.

https://doi.org/10.5194/amt-2020-65
Preprint. Discussion started: 27 May 2020

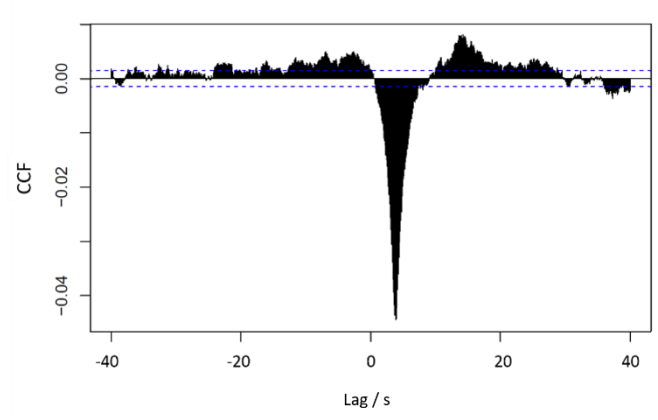

Figure 4: Example cross correlation function (CCF) for ozone and vertical wind on 10th April. The negative peak minimum indicates that ozone data lags 3.9 seconds behind the wind data.

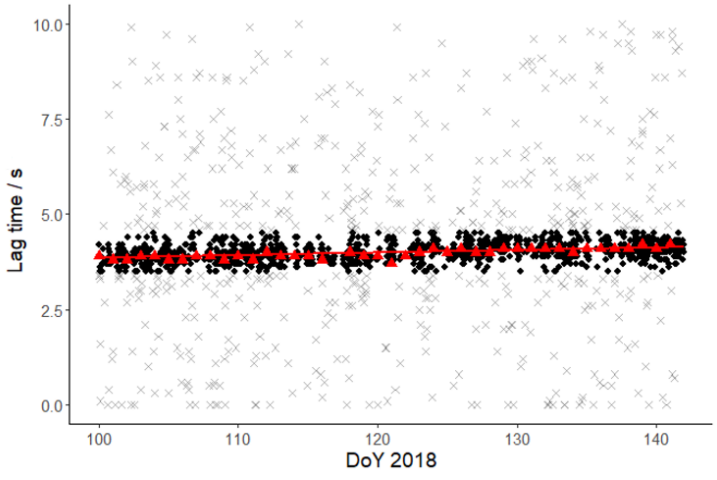

Figure 5: Lag times determined for each 20-minute period. Lags between 3.5 and 4.5 seconds (black dots) were accepted and used to plot a linear fit (red line). Determined lags outside of these bounds (grey crosses) were rejected, and were instead set to the linear fit. Lags determined from daily CCF are shown as red triangles.

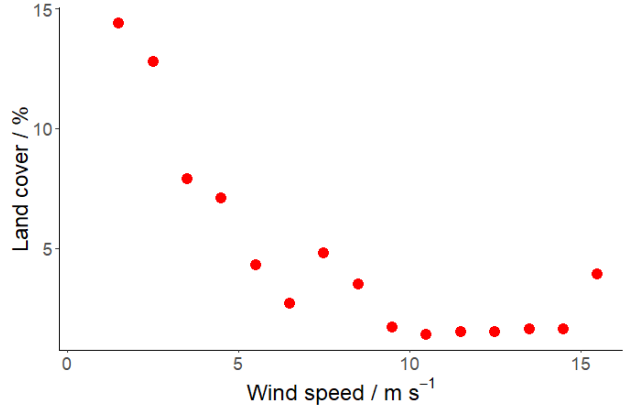

https://doi.org/10.5194/amt-2020-65
Preprint. Discussion started: 27 May 2020

Atmospheric Measurement Techniques Discussions

Figure 6: Land cover percentage within the average flux footprint for 1 m s^{-1} wind speed bins as calculated with the Kljun et al. (2015) flux footprint model.

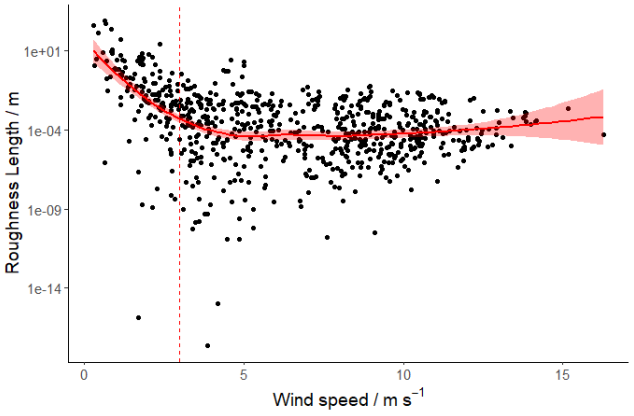

Figure 7: Roughness length for each averaging period, increased by land influence within the footprint at low wind speeds, with a smoothed line of fit (solid red) and the 3 m s^{-1} filter threshold (dashed red).

https://doi.org/10.5194/amt-2020-65
Preprint. Discussion started: 27 May 2020

Atmospheric Measurement Techniques Discussions

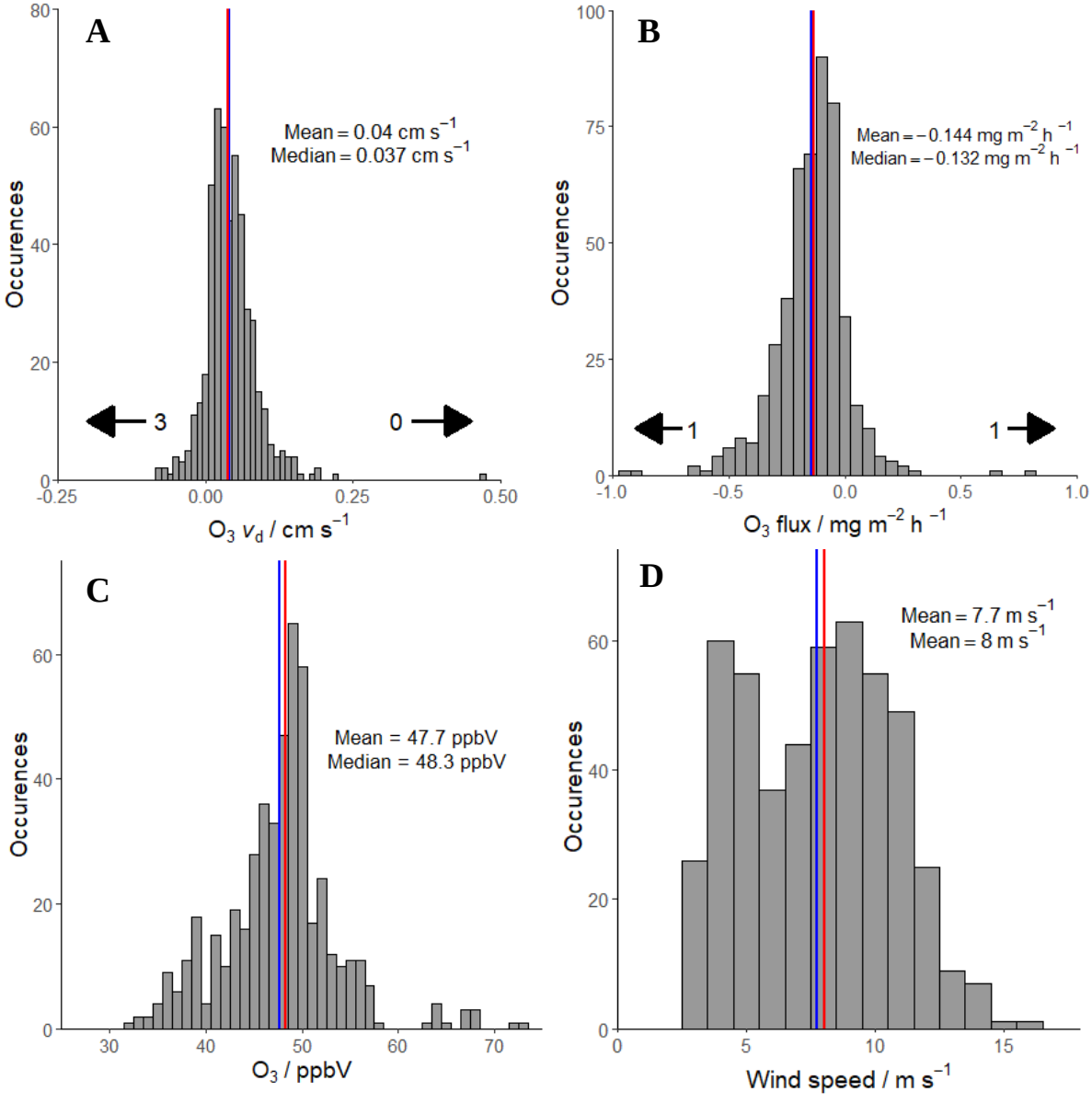

https://doi.org/10.5194/amt-2020-65
Preprint. Discussion started: 27 May 2020

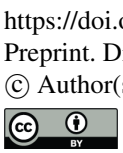

Atmospheric Measurement Techniques Discussions

Figure 8: Ozone deposition velocity (A), mass flux (B), ozone concentration (C) and wind speed (D) histograms for all periods that passed the filtering criteria. Mean values are represented by blue lines, median values by red lines. Deposition velocity and mass flux are plotted in the range -0.25 – 0.50 cm s^{-1} and -1.0 – 1.0 mg m^{-2} h^{-1} respectively for clarity, with arrows indicating the number of points beyond these limits.

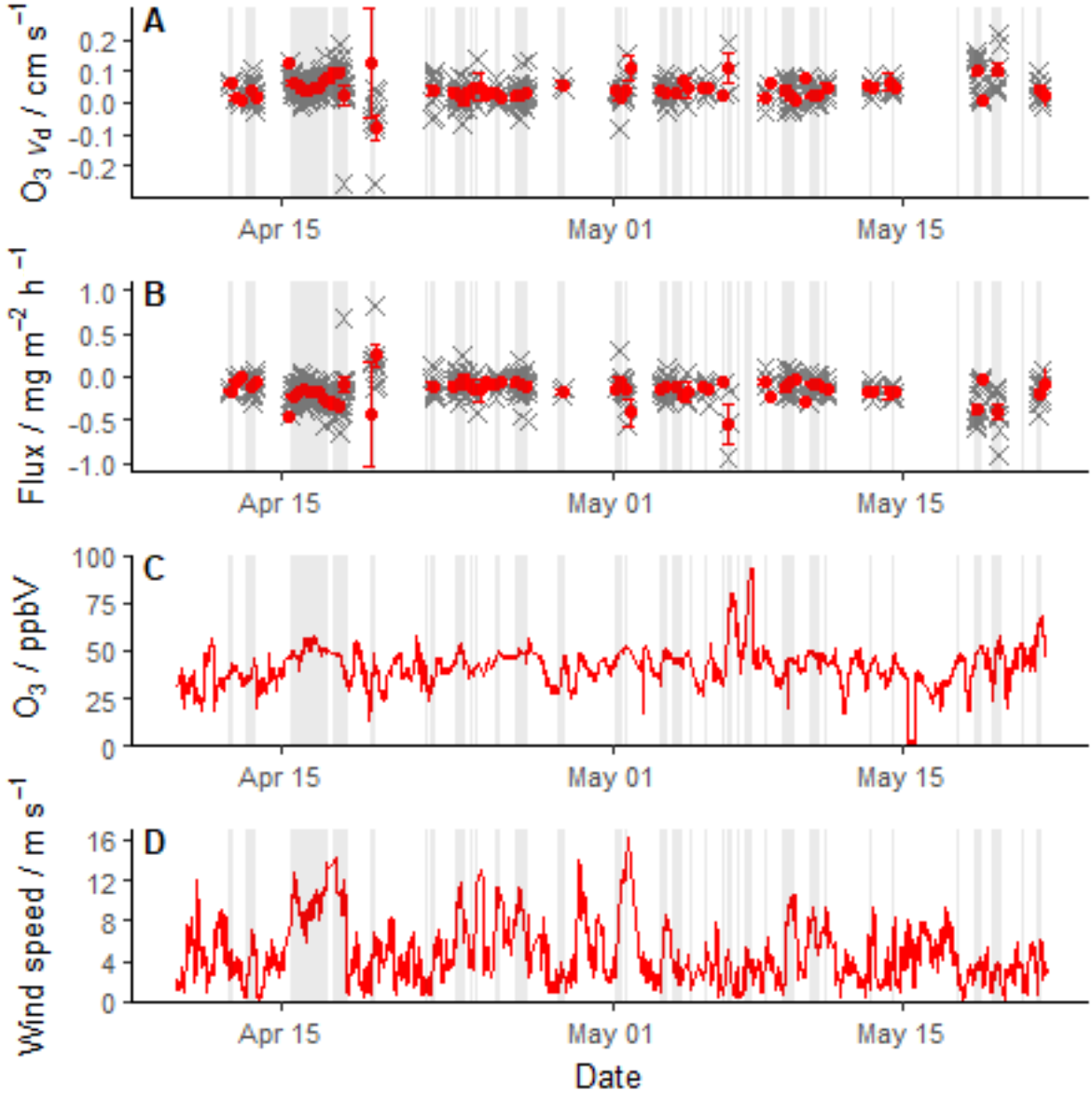

Figure 9: Timeseries of ozone deposition velocity (A), ozone mass flux (B), mean ozone concentration (C) and mean wind speed (D) from 10th April to 21st May 2018. Grey crosses represent 20-minute values, with red dots for 6-hour means with standard errors. All concentration and wind speed data are shown from 10th April to 21st May, with only deposition/flux values that passed filtering criteria shown in (A) and (B). Periods with an accepted wind direction (180-240°) are shaded. (A) and (B) are limited at ± 0.3 cm s^{-1} and ± 1 mg m^{-2} h^{-1} respectively for clarity. Points omitted are v_d = -0.442 (1.47 mg m^{-2} h^{-1}) and v_d = 0.472 (-1.64 mg m^{-2} h^{-1}), causing the large error bars on April 19th.

https://doi.org/10.5194/amt-2020-65
Preprint. Discussion started: 27 May 2020

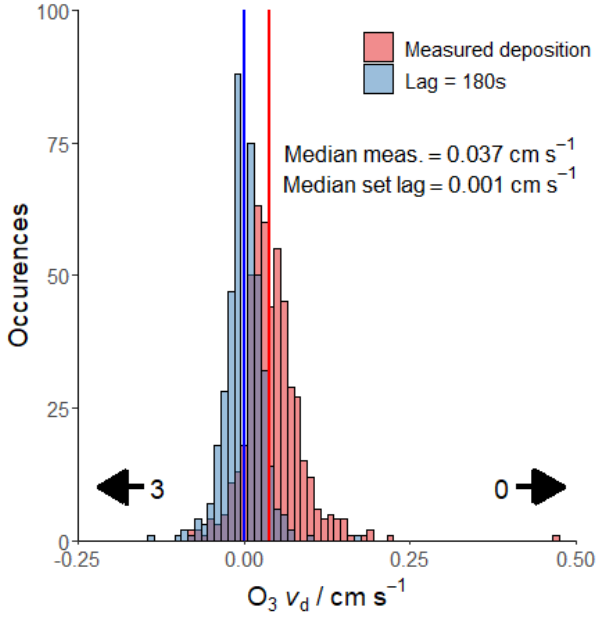

575 **Figure 10: Observed deposition velocity (red) vs deposition observed with lag = 180s (blue). Medians given by respectively coloured lines. X axis limited from -0.25 – 0.5 for clarity, with the number of points out of these bound indicated by the arrows**

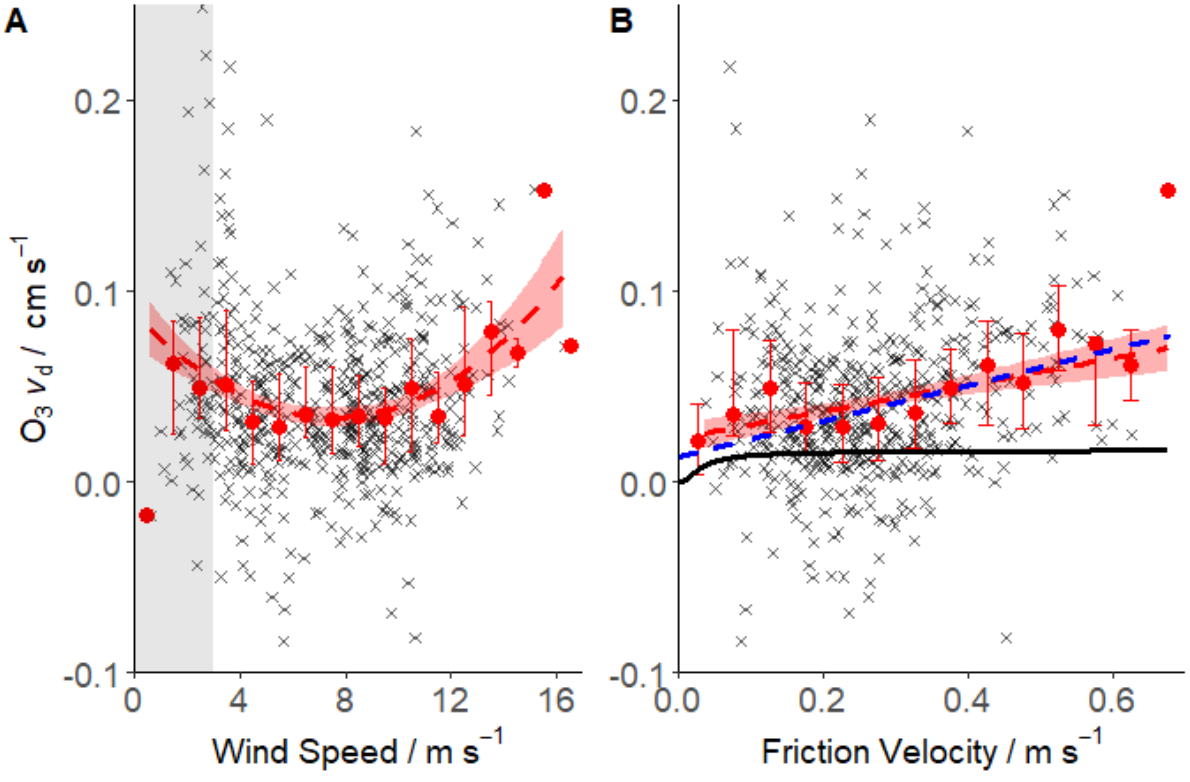

https://doi.org/10.5194/amt-2020-65
Preprint. Discussion started: 27 May 2020

Atmospheric Measurement Techniques Discussions

Figure 11: Deposition velocity dependence on wind speed (A) and friction velocity (B). 20-minute values are shown in grey, with bin-averaged medians (1 and 0.05 m s^{-1} respectively) with interquartile ranges shown in red. Wind speed dependence is presented with a 2nd order polynomial fit, with the grey region below 3 m s^{-1} indicating values removed by the wind speed filter (Sect. 4). Friction velocity dependence is presented with a linear fit in red, with the dependence predicted by Fairall et al. (2007) in blue and that predicted by Luhar et al. (2018) in black.

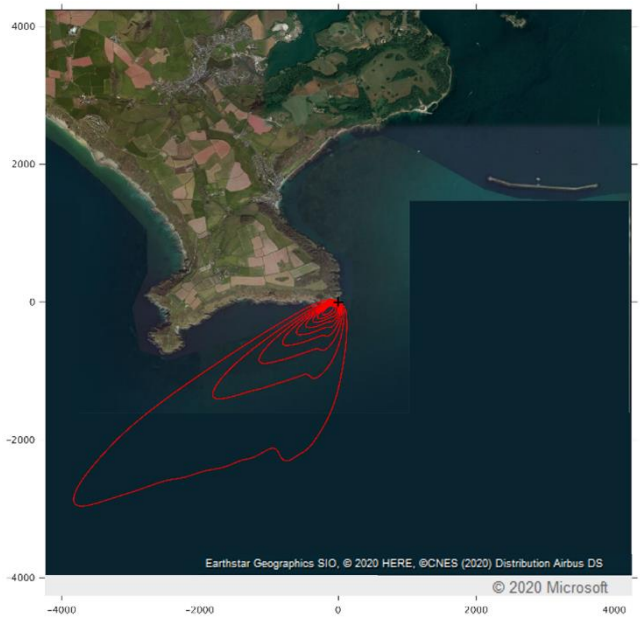

Figure 12: Flux footprint climatology for all 20-minute data that passed the selection criteria according to the Kljun et al. (2015) footprint model. A binary land/sea classification estimated a mean land contribution of 3.9%.

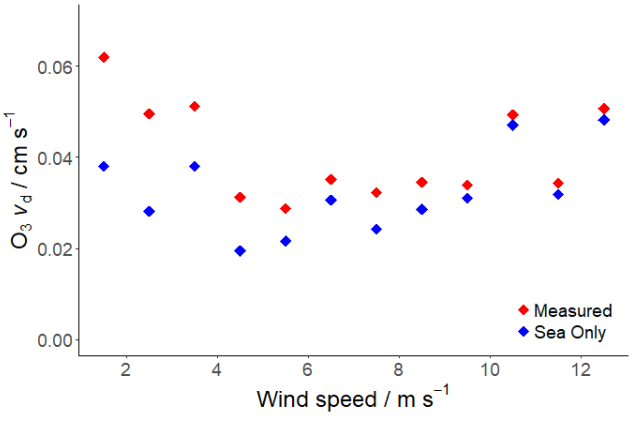

Figure 13: Median deposition velocities in 1 m s^{-1} wind speed bins for combined land and water surfaces as measured (red) and for water surfaces only (blue).

https://doi.org/10.5194/amt-2020-65
Preprint. Discussion started: 27 May 2020

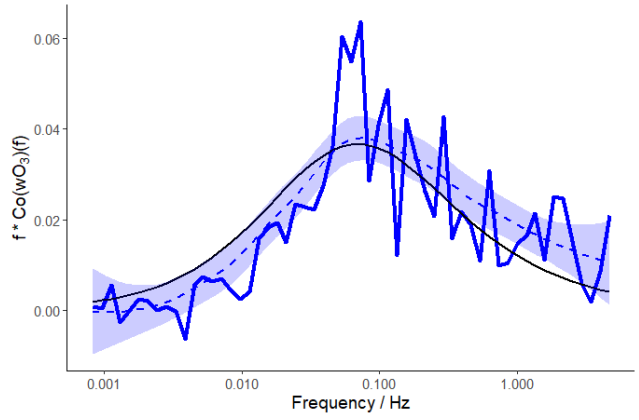

590

Figure 14: Average normalised ozone flux cospectrum for the 17th April. Wind speeds were 10.3 – 12.3 m s^{-1} and dimensionless Obukhov lengths were 0.14 – 0.17, representing near neutral, slightly stable conditions. Kaimal prediction shown in black.